Advances in Concrete Construction, *Vol. 9, No. 3 (2020) 289-299*
DOI: https://doi.org/10.12989/acc.2020.9.3.289

Experimental study on long-term behavior of RC columns subjected to sustained eccentric load

Chang-Soo Kim[1a], Yu Gong[2b], Xin Zhang[2c] and Hyeon-Jong Hwang*[3]

[1]*School of Architecture, Seoul National University of Science and Technology, 232 Gongreung-ro, Nowon-gu, Seoul 01811, Republic of Korea*
[2]*School of Civil Engineering, Shandong Jianzhu University, Shandong Provincial Key Laboratory of Appraisal and Retrofitting in Building Structures, Fengming Road, Lingang Development Zone, Jinan, Shandong, 250101, P.R. China*
[3]*School of Architecture, Konkuk University, 120 Neungdong-ro, Seoul 05029, Republic of Korea*

(*Received July 25, 2019, Revised January 15, 2020, Accepted February 13, 2020*)

Abstract. To investigate the long-term behavior of eccentrically loaded RC columns, which are more realistic in practice than concentrically loaded RC columns, long-term eccentric loading tests were conducted for 10 RC columns. Test parameters included concrete compressive strength, reinforcement ratio, bar yield strength, eccentricity ratio, slenderness ratio, and loading pattern. Test results showed that the strain and curvature of the columns increased with time, and concrete forces were gradually transferred to longitudinal bars due to the creep and shrinkage of concrete. The long-term behavior of the columns varied with the test parameters, and long-term effects were more pronounced in the case of using the lower strength concrete, lower strength steel, lower bar ratio, fewer loading-step, higher eccentricity ratio, and higher slenderness ratio. However, in all the columns, no longitudinal bars were yielded under service loads at the final measuring day. Meanwhile, the numerical analysis modeling using the ultimate creep coefficient and ultimate shrinkage strain measured from cylinder tests gave quite good predictions for the behavior of the columns.

Keywords: reinforced concrete column; long-term behavior; eccentric loading test; creep and shrinkage; minimum reinforcement

1. Introduction

In reinforced concrete (RC) columns, longitudinal bars provide resistance to bending (or tensile strength lacking in concrete), and in principle, longitudinal bars are designed so that the load-carrying capacity of a RC column is greater than strength-demands based on P-M interaction. However, the total area of longitudinal bars (A_s) or reinforcement ratio (ρ=A_s/A_g, where A_g=area of gross section) should satisfy the minimum reinforcement requirement specified in design codes: $\rho \geq \rho_{\min}$=1% in ACI 318 (2014) and KBC (2016), 0.8% in NZS 3101-2 (2017), 0.5-0.6% in GB 50010 (2015), or $A_s \geq A_{s,\min}=0.1N_{Ed}/f_{yd}$ ($A_{s,\min} \leq 0.002A_c$) in Eurocode 2 (2008) (where N_{Ed}=design axial compression force, f_{yd}=design yield strength of longitudinal bars, and A_c=area of concrete section).

The minimum requirement for longitudinal bars, which was first introduced in 1936 by ACI Committee 501, is to prevent longitudinal bars from yielding under sustained service loads (ACI 2014): in RC columns, concrete stress is gradually relaxed with time due to the creep and shrinkage of concrete, and the relaxed concrete stress is transferred to longitudinal bars, which may result in yielding of longitudinal bars even at service load levels (Gilbert 1988, Hamed and Lai 2016, Kim and Gong 2018).

However, because the current requirement was established based on the test results for concentrically loaded RC columns with low-strength materials, it could be neither safe nor economic in some cases (Ziehl *et al*. 1988, Kim and Gong 2018). In particular, as the eccentricity of axial loads and slenderness of columns increase, such premature bar yielding could be more pronounced because of highly stressed sections in part and 2nd-order effects (Lou *et al*. 2015, Kim and Gong 2018). To investigate the long-term behavior of eccentrically loaded RC columns, which are more realistic in practice than concentrically loaded RC columns, studies have been done, but as summarized in Table 1, only a few tests are available in the literature for the eccentrically loaded RC columns (Viest *et al*. 1956, Green and Breen 1969, Kordina 1972, Tatsa 1989, Claeson and Gylltoft 2000, Bradford 2005, Eom *et al*. 2018) due to difficulties in testing. Thus, more tests are required with a wide variety of design parameters.

In the present study, long-term eccentric loading tests were conducted for 10 RC columns with various test parameters, including concrete compressive strength (f_c' = 24.5 or 63.3 MPa), reinforcement ratio (ρ=0.60, 0.91, or 1.55%), bar yield strength (f_{yl}=321, 441, or 472 MPa), eccentricity ratio (e_0/D=0.1, 0.3, or 0.5), slenderness ratio (λ=21.5, 31.9, or 42.3), and loading pattern (1- or 2-step loading). The experimental study results were compared with numerical study results, and based on those study results, the minimum reinforcement was discussed.

*Corresponding author, Assistant Professor
E-mail: hwanggun85@naver.com
[a]Associate Professor
[b]Master Student
[c]Professor

http://www.techno-press.org/?journal=acc&subpage=7

ISSN: 2287-5301 (Print), 2287-531X (Online)

Table 1 Existing tests for RC columns under sustained eccentric axial loads

Authors		Viest *et al.* (1956)	Green and Breen (1969)	Kordina (1972)	Tatsa (1989)	Claeson and Gylltoft (2000)	Bradford (2005)	Eom *et al.* (2018)
Test parameters		f_c', e_0	e_0, P_{serv}	f_c', ρ, e_0, P_{serv}	NS	f_c'	Unequal Eccentricity	e_0, P_{serv}
No. of specimens		19	10	12	7	2	5	4
Concrete	f_c' (MPa)	15.7, 28.6, 33.6	22.9-37.9	26.2-46.0	29.1	35.5, 92.3	29.3	47.3
Longi -tudinal bars	f_{yl} (MPa)	298.5	386.1-451.6	261.4-453.3	NS	636	NS	NS
	ρ (%)	3.2	2.0	1.0, 2.3, 3.4	2.1	2.0	2.0	2.0
Section	$B\times D$ (mm)	127×127	152×102	264×171	300×145	200×200	150×150	200×300
Slender -ness	L (mm)	1016	1905	5145	2576	4100	5000	1010×2 (Cantilevered)
	λ	27.7	64.7	104.2	61.5	71.0	115.5	23.3
Service load	$\frac{P_{serv}}{P_{u,s}}$	0.80-0.95	0.37-0.79, 0.98	0.25-0.62	0.35	0.7, 0.8	NS (P_{serv}= 70-85 kN)	NS (P_{serv}= 421, 842 kN)
	$\frac{e_0}{D}$	0.25-0.76	0.04-0.42	0.14-0.50	0.345	0.1	0.333 at Top & ±0.333, ±0.167, 0 at Bottom	0.167
	Loading pattern	1-step	1-step	1-step	1-step	1-step, 2-step	1-step	1-step
Ambient conditions	T (°C)	18.3-28.9	18.5 (Avg)	20±1.5	NS	18±2	NS	8 (Avg)
	RH (%)	36-91	75 (Avg)	65±3	NS	30 (Avg)	NS	40 (Avg)
Remarks		SU				SU		

* f_c' = compressive strength of concrete, f_{yl}=yield strength of longitudinal bars, $\rho=A_s/A_g$=reinforcement ratio (A_s=total area of longitudinal bars, and A_g=area of gross section), B,D=width and depth of cross-section in the direction of bending, L=total column length between hinged ends, $\lambda=kL=r$=slenderness ratio k=1.0=effective length factor for hinged ends, $r=\sqrt{I_g / A_g}$ = radius of gyration, and I_g=moment of inertia of gross section) (ACI 2014), $P_{serv}/P_{u,s}$=service load level reported in the literature (P_{serv}=applied service load, and $P_{u,s}$=short-term ultimate strength of column), e_0/D=eccentricity ratio (e_0=initial eccentricity of axial load measured from centroid), T=temperature, RH=relative humidity, NS=not specified or not clearly stated in the literature, SU = short-term ultimate loading test after long-term loading, and Avg=on average. It is noted that there were minor differences in actual values, which are available in the literature.

2. Test plan

2.1 Test specimens

Fig. 1 shows the test specimens, and Table 2 summarizes the actual properties measured from the specimens. The cross-section was $B\times D$=260×200 mm in all columns (B=width and D=depth in the bending direction). In the control specimen S1, the specified compressive strength of concrete was f_c' = 24.5 MPa (C30). Six D10 bars of HRB400 in Chinese Standards (nominal diameter d_{sl1}=10 mm, nominal area A_{sl1}=78.54 mm^2, and measured yield strength f_{yl}=441 MPa) were used for longitudinal bars (reinforcement ratio $\rho=A_s/A_g$=0.91%, where $A_s=\sum A_{sl1}$=total area of longitudinal bars, and $A_g=B\times D$=gross area), and D10 bars were vertically spaced at s=200 mm for transverse bars (volumetric ratio of transverse bars to confined concrete $\rho_{st}=(A_{st,x}B_c+A_{st,y}D_c)/(sB_cD_c)$=0.90%, where $A_{st,x}=A_{st,y}$=total areas of transverse bars parallel to the directions of width and depth, and B_c, D_c=width and depth of confined concrete measured center-to-center of transverse bars). According to ACI 318 (2014), the slenderness ratio of the column was calculated as $\lambda=kL/r$=31.9 by using k=1.0 (effective length factor for hinged ends), L=1840 mm (total column length including top and bottom rigid end zones for eccentric loading), and $r=\sqrt{I_g / A_g}$ (radius of gyration, where I_g=moment of inertia of gross section), and the column was categorized as a slender column (when $\lambda\geq 22$ for non-sway columns). The service load of P_{serv}=235.8 kN was fully applied at t=28 days (i.e., 1-step loading) with a eccentricity ratio of e_0/D=0.3, which corresponded to $P_{serv}/P_{u,s}$=0.41 ($P_{u,s}$=short-term ultimate strength of the column specimen calculated by numerical analysis).

To investigate the effects of test parameters, f_c' = 63.3 MPa concrete (C80) was used in S2, f_{yl}=321 MPa steel (HRB335 in Chinese Standards) was used in S3, the reinforcement ratio was decreased to ρ=0.60% in S4 (four D10 bars) or increased to ρ=1.55% in S5 (four D16 bars of HRB400 in Chinese Standards: d_{sl1}=16 mm, A_{sl1}=201.1 mm^2, and f_{yl}=472 MPa). In S6, the column was loaded in two steps: the first and second half of P_{serv} were applied at t=28 and 35 days (1 week later). The eccentricity ratio was decreased to e_0/D=0.1 in S7 or increased to e_0/D=0.5 in S8,

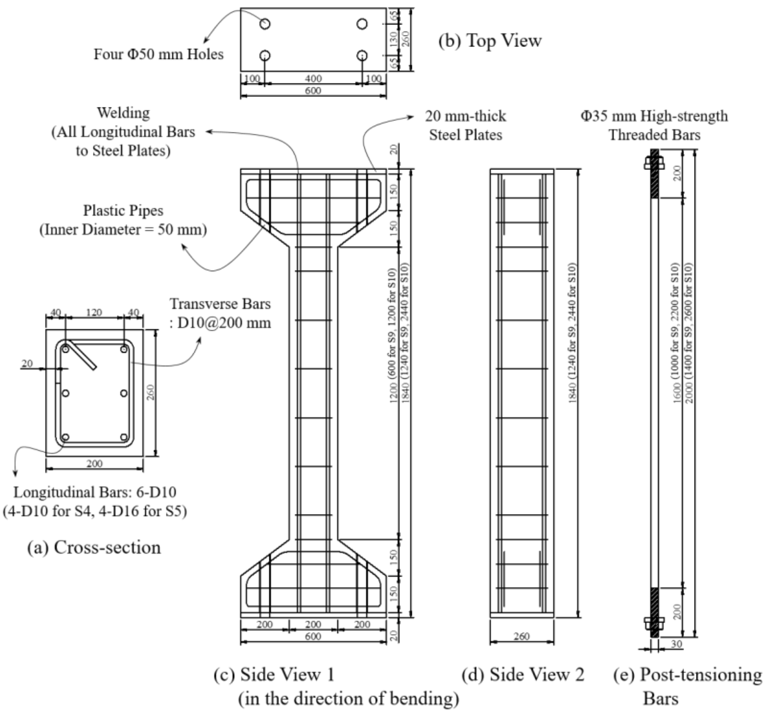

Fig. 1 Test specimens (units: mm)

Fig. 2 Production of test specimens

Table 2 Test specimens

Specimen		S1	S2	S3	S4	S5	S6	S7	S8	S9	S10
Parameter		Control	f_c'	f_{yl}	ρ	ρ	2-step Loading	$\frac{e_0}{D}$	$\frac{e_0}{D}$	λ	λ
Section	B×D (mm)	264×200	265×198	266×201	266×202	261×201	260×198	265×201	259×200	264×200	262×202
Slender -ness	L (mm)	1842	1844	1845	1841	1843	1842	1843	1840	1239	2438
	λ	31.9	32.3	31.8	31.6	31.8	32.2	31.8	31.9	21.5	41.8
Concrete	$f_c'(28)$ (MPa)	24.5	63.3	24.5	24.5	24.5	24.5	24.5	24.5	24.5	24.5
Longi -tudinal bars	f_{yl} (MPa)	441	441	321	441	472	441	441	441	441	441
	Arrange -ment (ρ)	6-D10 (0.91%)	6-D10 (0.91%)	6-D10 (0.91%)	4-D10 (0.60%)	4-D16 (1.55%)	6-D10 (0.91%)	6-D10 (0.91%)	6-D10 (0.91%)	6-D10 (0.91%)	6-D10 (0.91%)
Trans -verse bars	f_{yt} (MPa)	441	441	441	441	441	441	441	441	441	441
	Arrange -ment	D10@ 200 mm	D10@ 200 mm	D10@ 200 mm	D10@ 200 mm	D10@ 200 mm	D10@ 200 mm	D10@ 200 mm	D10@ 200 mm	D10@ 200 mm	D10@ 200 mm
Service load*	e_0/D	0.3	0.3	0.3	0.3	0.3	0.3	0.1	0.5	0.3	0.3
	P_{serv} (kN)	235.8	442.8	229.6	217.8	279.1	230.4	445.8	127.1	258.6	209.6
	$P_{serv}/P_{u,s}$**	0.41	0.41	0.41	0.41	0.41	0.41	0.41	0.41	0.41	0.41
	Loading pattern	1-step	1-step	1-step	1-step	1-step	2-step	1-step	1-step	1-step	1-step

* Service load was fully applied at t=28 days except for S6 (in S6, the half of P_{serv} was applied at t=28 days, and the other half was applied at t=35 days).
** Short-term ultimate strength of column $P_{u,s}$ was calculated by numerical analysis.

and the total column length was decreased to L=1240 mm in S9 (λ=21.5) or increased to L=2440 mm in S10 (λ=41.8).

2.2 Production of test specimens and ambient conditions

Fig. 2 shows the production sequence of test specimens. Both ends (or rigid end zones) of each column specimen were enlarged in section and strengthened with 20 mm-thick steel plates to avoid stress-concentration or local-failure during loading. Longitudinal bars were welded to the steel plates for anchorage, and plastic pipes (inner diameter =50 mm) were embedded in the rigid end zones to enable post-tensioning bars to pass through. All column specimens were cast horizontally, and then cured (covered with plastic) in that position. 2-3 days before loading, formwork was

Table 3 Mix and properties of concrete

Type	Materials per Unit Volume (kg/m^3)*										Properties of Fresh Concrete	
	W	*C*	*GGBS*	*FA*	*S*	*G*	*A*	*W/B* (%)	*S/a* (%)	*A/B* (%)	Slump (mm)	Air Content (%)
C30	185	440	-	-	700	1050	8.80	42.0	40.0	2.0	85	5.0
C80	150	460	50	90	680	1000	2.65	25.0	40.5	0.4	648**	2.0

* *W*=water, *C*=cement (42.5 cement for C30 or 52.5 cement for C80), GGBS=ground granulated blast-furnace slag, *FA*=fly ash and fine glass powder (60+30 kg/m^3 for C80), *S*=sand, *G*=gravel, *A*=water-reducing admixture and antifoaming agent (0.15 kg/m^3 for C80), *B*=Binders (C+GGBS+FA), and *a*=aggregates (S+G).
** Slump flow.

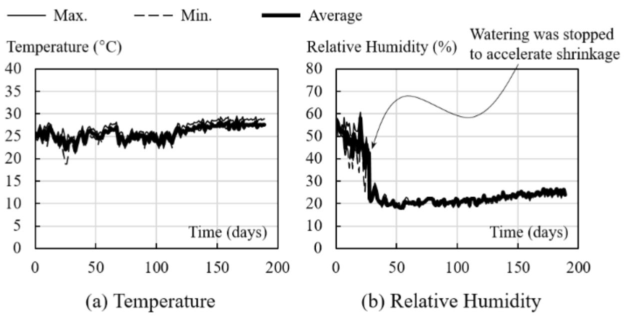

Fig. 3 Measured temperature and relative humidity

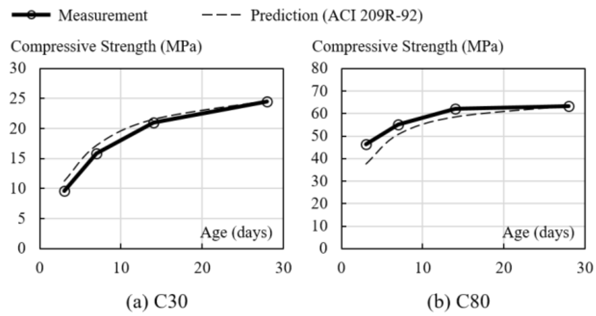

Fig. 4 Concrete strength development with time

removed, scaffolding was set up for safety, and then the column specimens were erected using a chain hoist (carefully erected to prevent cracking or other damages).

Long-term eccentric loading tests were conducted in a room on the ground floor, and loading was sustained for 160 days (t=188 days) after the first loading (t=28 days). To minimize strain-variations due to temperature changes, controlled heating (by an automatic room heater and hot-air blowers) was provided until the end of testing. Controlled watering (by humidifiers and an automatic floor watering device) was also provided for curing before loading, but stopped after loading to accelerate shrinkage.

The ambient temperature and humidity were measured by digital equipment, and the measured values are shown in Fig. 3: during test, the mean and standard deviation was T=25.8±1.5°C for the temperature or RH=22.1±2.1% for the relative humidity after loading (before loading, RH=48.4±5.3%).

2.3 Materials

Table 3 presents the mix design of concrete. Concrete mixtures were proportioned for $f_c' =$ 30 MPa (C30) and 80 MPa (C80), and the maximum aggregate size was 20 mm.

To measure compressive strength and shrinkage and creep strains of concrete, 16 concrete cylinders (Φ150×300 mm) were prepared for each mixture (12 for compressive strength tests at t=3, 7, 14, and 28 days, 2 for shrinkage tests, and 2 for creep tests). For consistency in the ambient conditions, the concrete cylinders were cast, cured, and stripped from molds together with the column specimens in the same room at the same time.

Compressive strength tests were carried out for concrete cylinders according to ASTM C39/C39M (2018). At the age of 28 days, the average cylinder compressive strength and modulus of elasticity measured $f_c'(28) =$ 24.5 MPa and E_c (28)=23.0 GPa for C30 or 63.3 MPa and 30.9 GPa for C80. Fig. 4 shows the development of concrete strength with time, and compares the measured values with the predictions by the maturity model of ACI 209R-92 (1997): $f_c'(t) = f_c'(28) \times t / (\alpha + \beta t)$, where t=concrete age in days and α, β=constants for Type I cement (4.0 and 0.85 for C30) or Type III cement (2.3 and 0.92 for C80).

Direct tension tests were also carried out for reinforcing bars according to ASTM E8/E8M (2016). The average modulus of elasticity, yield strength, and ultimate tensile strength were E_s=195 GPa, f_y=441.3 MPa, and f_u=486.0 MPa for HRB400 D10 bars, E_s=203 GPa, f_y=472.1 MPa, and f_u=608.5 MPa for HRB400 D16 bars, or E_s=198 GPa, f_y=320.5 MPa, and f_u=450.3 MPa for HRB335 D10 bars.

2.4 Loading and measurement

The service loading was applied on each column specimen through four post-tensioning bars (Fig. 5): two in compression (or concave) side and another two in tension (or convex) side. To minimize the number of post-tensioning bars and to ensure the bars remain elastic after tensioning, large-diameter and high-strength steel bars were used (diameter=35 mm and yield strength $f_{y,pt}$=600 MPa). The tensioned bars were bolted only at the outside of each column specimen to eliminate the contribution of the bars to the time-dependent deformation of the column specimen. The rigid end zones at both ends transfer forces from the post-tensioning bars (in tension) to the column (in compression).

The service load level was determined based on the

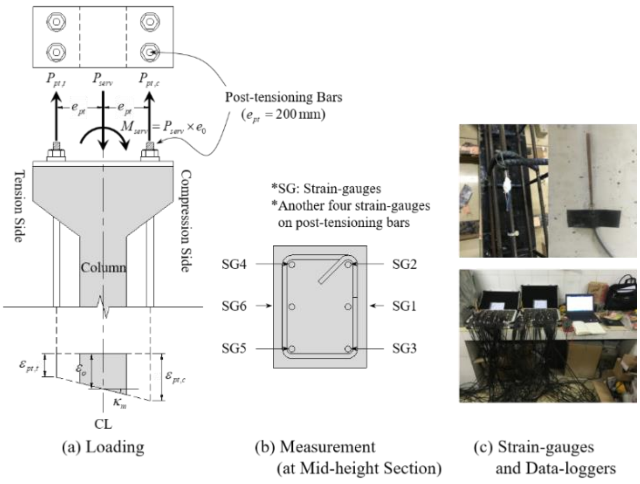

Fig. 5 Loading and measurement

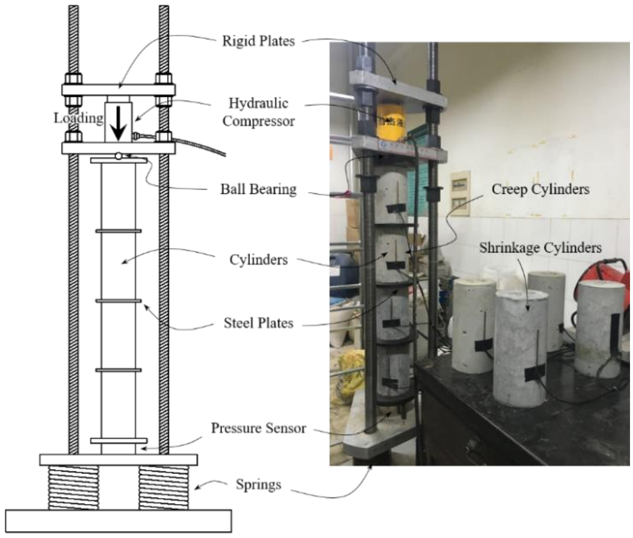

Fig. 6 Creep and shrinkage tests for concrete cylinders

design considerations of ACI 318 (2014) as given in Eq. (1).

$$1.2D + 1.6L = \Phi P_{u,s} \tag{1a}$$

$$D = \frac{\Phi}{1.2 + 1.6X} P_{u,s} = P_{serv} \tag{1b}$$

where D,L=dead and live loads (X=L/D=live-to-dead load ratio), Φ=strength reduction factor, $P_{u,s}$=short-term ultimate strength of column, and P_{serv}=long-term service load. In the present study, X=0.25 and Φ=0.65 (compression-controlled sections for other reinforced members (ACI 2014)) were assumed, which resulted in P_{serv}=0.41$P_{u,s}$, and the short-term ultimate strength $P_{u,s}$ of each column specimen was calculated by numerical analysis.

The required post-tensioning forces, which are to generate the service load P_{serv} with an initial eccentricity e_0 of axial load (or bending moment M_{serv}=P_{serv}×e_0 at column ends) on each column specimen, were calculated using Eq. (2) based on the force equilibrium and linear strain distribution assumption (Kim *et al*. 2017).

$$P_{serv} = P_{pt,c} + P_{pt,t} \tag{2a}$$

$$M_{serv} = P_{serv} \times e_0 = \left(P_{pt,c} - P_{pt,t}\right) \times e_{pt} \tag{2b}$$

$$P_{pt,c} = P_{serv} \frac{\left(1 + e_0 / e_{pt}\right)}{2} \tag{2c}$$

$$P_{pt,c} = P_{serv} \frac{\left(1 - e_0 / e_{pt}\right)}{2} \tag{2d}$$

where $P_{pt,c}$, $P_{pt,t}$=total post-tensioning forces at compression and tension sides, and e_{pt}=200 mm=eccentric distance of post-tensioning forces.

The post-tensioning forces were applied by fastening nuts using a high-capacity pneumatic wrench. Since the tensioned bars remained elastic, the service load can be controlled by maintaining the initial strain of the bars to compensate for the loss in service due to the creep and shrinkage of concrete. The required tensile strain of post-tensioning bars at both sides can be calculated using Eq. (3) (Kim *et al*. 2017).

$$\varepsilon_{pt,c} = \frac{P_{pt,c}}{EA_{pt,c}} \tag{3a}$$

$$\varepsilon_{pt,t} = \frac{P_{pt,t}}{EA_{pt,t}} \tag{3b}$$

where $EA_{pt,c}$, $EA_{pt,c}$=total axial stiffnesses of post-tensioning bars at compression and tension sides.

Since post-tensioning bars interacted with each other during fastening, the post-tensioning bars were carefully tensioned in this sequence: 1) all nuts were tightened manually; 2) two bars at the compression side were tensioned up to one-third of the required strain; 3) two bars at the tension side were tensioned up to one-third of the required strain; 4) the steps 2 and 3 were repeated until all bars reached the required strains; and 5) bar strains were adjusted minutely. The strain of post-tensioning bars was continually adjusted (or load-adjustment) with a tolerance of initial value ±50μ, daily up to the first week after loading, weekly for the following first month, and monthly until the end of testing (additional load-adjustments were made when large changes in strain were observed). The strain of post-tensioning bars was read before and after every load-adjustment, and strain-measurement and load-adjustment were made at a similar time (around 10:00 AM) for consistency.

To measure strains at the mid-height section, 10 strain-gauges were installed for each column specimen (Fig. 5): 2 on concrete (installed one day before loading, after removal of formwork), 4 on reinforcing bars, and 4 on post-tensioning bars. Shrinkage before loading was ignored and strain-measurement was started from 28 days (at the day of loading). For data reading from 118 strain-gauges (10 for each column specimen and total 10 column specimens, 2 for each cylinder specimen and total 8 cylinder specimens, and two for temperature compensation of concrete and steel), two data-loggers were used.

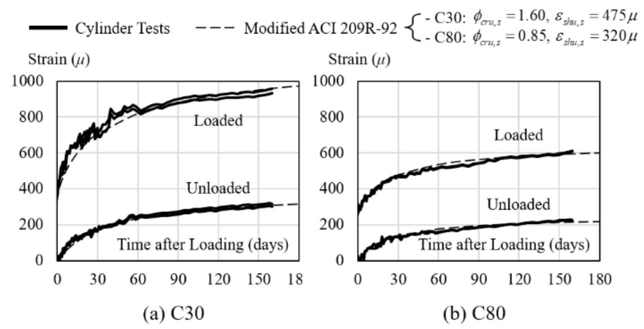

Fig. 7 Cylinder test results

3. Test results

3.1 Cylinder tests

Creep and shrinkage tests were carried out for concrete cylinders according to ASTM C512/C512M (2015). Two creep cylinders for each mixture were initially loaded at the age of 28 days through a 500 kN creep frame (Fig. 6). The stress applied to the cylinders corresponded to $\sigma_{serv}=0.31f_c'$ for C30 or $0.12f_c'$ for C80. Although the stress levels are lower than the general case of $0.4f_c'$, the same creep coefficient can be applicable to cylinders, which are under the same ambient conditions and subjected to stresses lower than $0.4f_c'$ (Kim 2003, ASTM 2015).

Thick solid lines in Fig. 7 are the measured strains from the unloaded and loaded cylinder specimens. The measured strains gradually increased with time, and at t=188 days (or 160 days after loading), the average strain obtained from the two unloaded cylinders (involving shrinkage strain only) was 312 μ for C30 or 228 μ for C80, and the average strain obtained from the two loaded cylinders (involving instantaneous, creep, and shrinkage strains) was 945 μ for C30 or 609 μ for C80.

To evaluate the ultimate creep coefficient ϕ_{cru} and ultimate shrinkage strain ε_{shu} of concrete based on the prediction model of ACI 209R-92 (1997), the predictions were calibrated to the cylinder test results. In the predictions, the proposed modifications of Huo *et al*. (2001) were also implemented to consider characteristics of high-strength concrete (detailed descriptions are available in Kim and Gong 2018), and correction factors for other than standard conditions were calculated based on the following conditions: moist curing duration=28 days, relative humidity=22.1%, slump=85 mm for C30 or 210 mm for C80, fine aggregate ratio=40.0% for C30 or 40.5% for C80, cement content=440 kg/m^3 for C30 or 600 kg/m^3 for C80 (including cement, slag, fly ash, and glass powder), air content=5% for C30 or 2% for C80, and concrete stress ratio=0.31 for C30 or 0.12 for C80. From the calibration of prediction to test, the ultimate creep coefficient $\phi_{cru,s}$ and ultimate shrinkage strain $\varepsilon_{shu,s}$ under standard conditions were evaluated as 1.60 and 475 μ for C30 or 0.85 and 320 μ for C80 (thin dashed lines in Fig. 7). The evaluated values were higher in C30 than in C80 as expected, and were smaller than the recommendation of ACI 209R-92 (1997) ($\phi_{cru,s}$=2.35 and $\varepsilon_{shu,s}$=780 μ in the absence of specific creep and shrinkage data).

It is noted that fluctuations in the measured strains were mainly attributed to temperature and humidity changes due to occasional opening and closing of the test room.

3.2 Column tests

Fig. 8 shows the column specimens being tested in the room, and Fig. 9 shows the measured strains $\varepsilon_{c,c}(t)$, $\varepsilon_{c,t}(t)$=concrete strains at compression and tension sides, and $\varepsilon_{s,c}(t)$, $\varepsilon_{s,t}(t)$= steel strains at compression and tension sides), measured curvature ($\kappa_m(t)$=average of $[\varepsilon_{c,c}(t)+\varepsilon_{c,t}(t)]/d_c$ and $[\varepsilon_{s,c}(t)+\varepsilon_{s,t}(t)]/d_s$, where $d_c=D$ and $d_s=D-40$ mm are distances between two opposite strain-gauges on concrete and steel), and calculated forces acting on structural components ($P_c(t)$, $P_s(t)$=concrete and steel forces) at the mid-height section (in the figure, shapes are test results, while lines are numerical analysis results which will be discussed in the next section).

If a material remains its elastic range after loading, its stress distribution can be defined by using the strain distribution and Hooke's law. Thus, the steel force $P_s(t)$ can be calculated by integrating stresses over the section of longitudinal bars (Eq. (4a)), and the concrete force $P_c(t)$ can be calculated by subtracting the steel force from the service load (Eq. (4b)) (Kim *et al*. 2017).

$$P_{sl}(t)=\Sigma\varepsilon_s(t)E_{sl}A_{sl} \tag{4a}$$

$$P_c(t)=P_{serv}-P_{sl}(t) \tag{4b}$$

The actual service load (P_{serv} and M_{serv} at column ends) and eccentricity ratio (e_0/D at column ends) were calculated by using Eqs. (2), (3), (4), and (5) and the measured strains.

Fig. 8 Column specimens

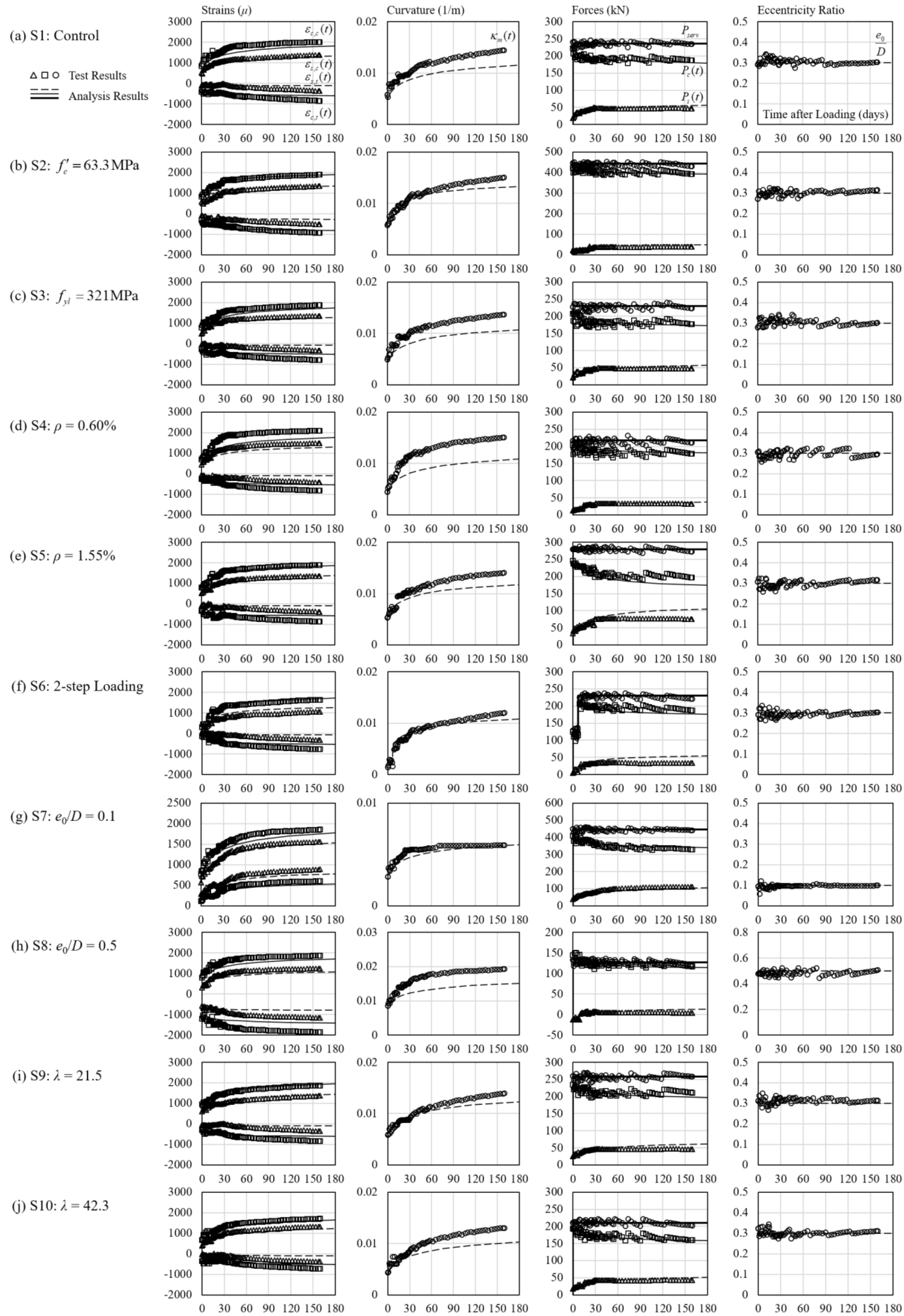

Fig. 9 Comparison of test and analysis results

$$e_0 / D = (M_{serv} / P_{serv}) / D \tag{5}$$

As shown in Fig. 9, the measured strains and curvatures ($\varepsilon_{c,c}(t)$, $\varepsilon_{c,t}(t)$, $\varepsilon_{s,c}(t)$, $\varepsilon_{s,c}(t)$, and $\kappa_m(t)$) generally increased with time, and gradual force-redistributions from concrete to longitudinal bars ($P_c(t)$ and $P_s(t)$) were observed. Although there were some fluctuations, the actual service load and eccentricity ratio (P_{serv} and e_0/D) were relatively consistent and close to the planned. The fluctuations were attributed to increments of creep and shrinkage strains with time and changes of ambient temperature and humidity between load-adjustments.

More specifically, in the control specimen S1 with P_{serv}=235.8 kN (Fig. 9(a)), the steel strain at the compression side (in the case, the steel strain was greater at the compression side than at the tension side), curvature, and steel force were $\varepsilon_{s,c}(t)$=1389 μ, $\kappa_m(t)$=0.0145 m^{-1}, and $P_{sl}(t)$=46.7 kN at t=188 days (160 days after loading). Compared to initial values measured at the day of loading ($\varepsilon_{s,c}(28)$=517 μ, $\kappa_m(28)$=0.0058 m^{-1}, and $P_{sl}(28)$=18.5 kN), the steel strain, curvature, and steel force were increased by $\Delta\varepsilon_{s,c}(t)/\varepsilon_{s,c}(28)$=168%, $\Delta\kappa_m(t)/\kappa_m(28)$=150%, and $\Delta P_{sl}(28)/P_{sl}(28)$=152%, respectively. However, the steel strain ($\varepsilon_{s,c}(t)$=1389 μ) was smaller than the yield strain (ε_{yl}=f_{yl}/E_{sl}=2263 μ).

In S2 with the higher strength concrete (f_c' = 63.3 MPa and P_{serv}=442.8 kN), $\varepsilon_{s,c}(t)$=1344 μ, $\kappa_m(t)$=0.0150 m^{-1}, $P_{sl}(t)$=38.0 kN, $\Delta\varepsilon_{s,c}(t)/\varepsilon_{s,c}(28)$=133%, $\Delta\kappa_m(t)/\kappa_m(28)$=159%, and $\Delta P_{sl}(28)/P_{sl}(28)$=75% (Fig. 9(b)). Even under the higher service load (188% of S1), the long-term effect in S2 was much less pronounced than in S1. This is because high-strength concrete shows smaller creep and shrinkage (ACI 1997, Huo *et al*. 2001).

In S3 with the lower strength steel (f_{yl}=320.5 MPa and P_{serv}=229.6 kN), $\varepsilon_{s,c}(t)$=1352 μ, $\kappa_m(t)$=0.0137 m^{-1}, $P_{sl}(t)$=46.4 kN, $\Delta\varepsilon_{s,c}(t)/\varepsilon_{s,c}(28)$=175%, $\Delta\kappa_m(t)/\kappa_m(28)$=181%, and $\Delta P_{sl}(28)/P_{sl}(28)$=130% (Fig. 9(c)). Although the overall behavior was similar to S1, the steel strain ($\varepsilon_{s,c}(t)$=1352 μ) was closer to the yield strain (ε_{yl}=1619 μ).

In S4 with the lower bar ratio (ρ=0.60% and P_{serv}=217.8 kN), $\varepsilon_{s,c}(t)$=1487 μ, $\kappa_m(t)$= 0.0151 m^{-1}, $P_{sl}(t)$=32.4 kN, $\Delta\varepsilon_{s,c}(t)/\varepsilon_{s,c}(28)$=234%, $\Delta\kappa_m(t)/\kappa_m(28)$=237%, and $\Delta P_{sl}(28)/P_{sl}(28)$=175% (Fig. 9(d)). As expected, the long-term effect was more pronounced with the decrease of the bar ratio.

In S5 with the higher bar ratio (ρ=1.55% and P_{serv}=279.1 kN), $\varepsilon_{s,c}(t)$=1238 μ, $\kappa_m(t)$=0.0123 m^{-1}, and $P_{sl}(t)$=77.5 kN (Fig. 9(e)). Even under the higher service load (118% of S1), the long-term effect was less pronounced ($\Delta\varepsilon_{s,c}(t)/\varepsilon_{s,c}(28)$=140%, $\Delta\kappa_m(t)/\kappa_m(28)$=130%, and $\Delta P_{sl}(28)/P_{sl}(28)$=130%). The higher area and the higher rigidity of longitudinal bars (ρ=1.55% and E_s=203 GPa in S5, but ρ=0.91% and E_s=195 GPa in S1) were mainly responsible for the smaller long-term effect in S5.

In S6 with the two-step loading (0.5P_{serv} at 28 days and 1.0P_{serv} at 35 days, and P_{serv}=230.4 kN), $\varepsilon_{s,c}(t)$=925 μ, $\kappa_m(t)$=0.0098 m^{-1}, and $P_{sl}(t)$=34.8 kN (Fig. 9(f)). Since the concrete in S6 was subjected to lower stresses at early ages between the first and second loadings, the long-term effect in S6 was smaller than in S1. This result implies that the practical design assumption (the service load fully applies and remains constant ignoring actual construction sequences) provides conservative design results (Kim and Gong 2018).

In S7 with the lower eccentricity ratio (e_0/D=0.1 and P_{serv}=445.8 kN), $\varepsilon_{s,c}(t)$=1448 μ, $\kappa_m(t)$=0.0058 m^{-1}, $P_{sl}(t)$=102.0 kN, $\Delta\varepsilon_{s,c}(t)/\varepsilon_{s,c}(28)$=153%, $\Delta\kappa_m(t)/\kappa_m(28)$=108%, and $\Delta P_{sl}(28)/P_{sl}(28)$=157% (Fig. 9(g)). Compared to S1, the increments in the steel strain and steel force were higher but the increment in the curvature was smaller, due to the lower eccentricity and higher compression.

In S8 with the higher eccentricity ratio (e_0/D=0.5 and P_{serv}=127.1 kN), $\varepsilon_{s,c}(t)$=1142 μ, $\kappa_m(t)$=0.0178 m-1, $P_{sl}(t)$=4.8 kN, $\Delta\varepsilon_{s,c}(t)/\varepsilon_{s,c}(28)$=277%, $\Delta\kappa_m(t)/\kappa_m(28)$=107%, and $\Delta P_{sl}(28)/P_{sl}(28)$=-140% (the steel force was in tension at the initial loading, but gradually increased and changed into compression) (Fig. 9(h)). Even under the much lower service load (54% of S1), the long-term effect was more significant with the increase of the eccentricity ratio.

In S9 with the lower slenderness ratio (λ=21.5 and P_{serv}=258.6 kN), $\varepsilon_{s,c}(t)$=1193 μ, $\kappa_m(t)$=0.0117 m^{-1}, $P_{sl}(t)$=46.1 kN, $\Delta\varepsilon_{s,c}(t)/\varepsilon_{s,c}(28)$=99%, $\Delta\kappa_m(t)/\kappa_m(28)$=99%, and $\Delta P_{sl}(28)/P_{sl}(28)$=85% (Fig. 9(i)). On the other hand, in S10 with the higher slenderness ratio (λ=41.8 and P_{serv}=209.6 kN), $\varepsilon_{s,c}(t)$=1152 μ, $\kappa_m(t)$=0.0109 m^{-1}, $P_{sl}(t)$=41.1 kN, $\Delta\varepsilon_{s,c}(t)/\varepsilon_{s,c}(28)$=189%, $\Delta\kappa_m(t)/\kappa_m(28)$=154%, and $\Delta P_{sl}(28)/P_{sl}(28)$=143% (Fig. 9(j)). Even allowing for the different service loads, the long-term effect was increased with the increase of the second-order effect.

4. Discussions

4.1 Numerical analysis

Using the numerical analysis modeling of Kim and Gong (2018) and the ultimate creep coefficient and ultimate shrinkage strain evaluated from the concrete cylinders, numerical analysis was performed for the column specimens. Fig. 9 compares the test (shapes in the figure) and analysis (lines in the figures) results, and Table 4 summarizes the comparison. Although there were some fluctuations in the actual service load and eccentricity ratio applied to the column specimens, as shown in the figure and table, the numerical analysis gave quite good predictions (at the final measuring day, the mean and standard deviation of prediction-to-test ratios=0.92±0.34). This result indicates that, if concrete cylinder test results are available, the long-term behavior of RC columns can be predicted with reasonable precision (Kataoka and Bittencourt 2014, Kim and Gong 2018).

It is noted that, in the cases of S4 with the lower bar ratio (ρ=0.60%) and S8 with the higher eccentricity ratio (e_0/D=0.5), due to vulnerability to deformation and cracking during the initial loading, it was hard to attain the service load and eccentricity ratio as planned. Thus, the discrepancy of prediction was relatively higher in S4 (prediction-to-test =0.83±0.28) and S8 (1.13±0.75). Meanwhile, the predictions for tension strains (0.72±0.09 for $\varepsilon_{s,t}$, and

Table 4 Comparison of test and analysis results at the final measuring day

Speci -men	T/P	$\varepsilon_{c,c}$ (μ)	$\varepsilon_{s,c}$ (μ)	$\varepsilon_{s,t}$ (μ)	$\varepsilon_{c,t}$ (μ)	κ_m (1/m)	P_{serv} (kN)	P_c (kN)	P_s (kN)	e_0/D	M ±SD
S1	T	2015	1389	-372	-847	0.014	234.2	187.5	46.7	0.30	0.86 ±0.26
	P	1797	1321	-107	-583	0.012	235.8	180.5	55.3	0.30	
	P/T	0.89	0.95	0.29	0.69	0.82	1.01	0.96	1.18	0.99	
S2	T	1897	1344	-517	-932	0.015	429.9	391.9	38.0	0.32	0.95 ±0.19
	P	1875	1331	-275	-820	0.014	442.8	394.2	48.6	0.30	
	P/T	0.99	0.99	0.53	0.88	0.91	1.03	1.01	1.28	0.95	
S3	T	1876	1352	-342	-807	0.014	223.0	175.8	47.2	0.30	0.85 ±0.29
	P	1707	1266	-69	-510	0.011	229.6	173.6	56.0	0.30	
	P/T	0.91	0.94	0.20	0.63	0.81	1.03	0.99	1.19	1.00	
S4	T	2089	1487	-428	-828	0.015	210.6	178.2	32.4	0.29	0.83 ±0.28
	P	1734	1284	-89	-539	0.011	217.8	181.4	36.4	0.30	
	P/T	0.83	0.86	0.21	0.65	0.75	1.03	1.02	1.12	1.02	
S5	T	1885	1350	-388	-866	0.014	272.0	193.4	78.6	0.32	0.88 ±0.29
	P	1843	1362	-96	-578	0.012	279.1	176.1	103.0	0.30	
	P/T	0.98	1.01	0.25	0.67	0.86	1.03	0.91	1.31	0.95	
S6	T	1642	1060	-328	-775	0.012	220.7	187.1	33.6	0.30	0.96 ±0.37
	P	1690	1244	-72	-518	0.011	230.4	176.5	53.9	0.30	
	P/T	1.03	1.17	0.22	0.67	0.93	1.04	0.94	1.61	0.99	
S7	T	1854	1558	888	604	0.006	441.4	329.0	112.4	0.10	0.96 ±0.07
	P	1751	1506	764	519	0.006	445.8	341.2	104.6	0.10	
	P/T	0.94	0.97	0.86	0.86	1.04	1.01	1.04	0.93	1.01	
S8	T	1862	1243	-1153	-1850	0.019	121.1	117.0	4.1	0.51	1.13 ±0.75
	P	1688	1069	-789	-1408	0.015	127.1	114.3	12.8	0.50	
	P/T	0.91	0.86	0.68	0.76	0.80	1.05	0.98	3.11	0.99	
S9	T	1866	1365	-351	-845	0.014	257.8	211.2	46.6	0.31	0.91 ±0.28
	P	1927	1420	-98	-605	0.013	258.6	198.4	60.2	0.30	
	P/T	1.03	1.04	0.28	0.72	0.91	1.00	0.94	1.29	0.95	
S10	T	1704	1316	-381	-731	0.013	202.5	159.6	42.9	0.31	0.87 ±0.27
	P	1627	1202	-95	-520	0.011	209.6	159.0	50.6	0.30	
	P/T	0.95	0.91	0.25	0.71	0.82	1.04	1.00	1.18	0.96	
M±SD		0.95 ±0.06	0.97 ±0.09	0.38 ±0.23	0.72 ±0.09	0.86 ±0.08	1.03 ±0.02	0.98 ±0.04	1.42 ±0.62	0.98 ±0.03	0.92 ±0.34

* T=test, P=prediction, and M±SD=mean and standard deviation of prediction-to-test ratios.

0.38±0.23 for $\varepsilon_{s,t}$) and curvatures (0.86 ± 0.08 for κ_m) were less accurate than those for compression strains (0.95±0.06 for $\varepsilon_{c,c}$, and 0.97±0.09 for $\varepsilon_{s,c}$) and forces (0.98±0.04 for P_c, and 1.23±0.18 for P_s except S8 (1.42±0.62 including S8)). Actual tensile creep and time-dependent cracking were appeared to be responsible for those inaccuracies (in the numerical analysis modeling, creep behavior in tension was assumed to be similar to that in low level compression (Gilbert 1988, Kim and Gong 2018).

4.2 Minimum reinforcement

The long-term behavior of RC members is strongly affected by reinforcement ratios (Kataoka and Bittencourt 2014, B-Jahromi *et al*. 2017, Kim and Gong 2018, Sun *et al*. 2019). In all the column specimens, no longitudinal bars were yielded under service loads at the final measuring day. The ratio of the measured steel strain (at the compression side) to the yield strain was just $\varepsilon_{s,c}(t)/\varepsilon_{yl}$=1% in S1 ($\rho$=0.91%), 59% in S2 ($\rho$=0.91%), 66% in S4 ($\rho$=0.60%), 53% in S5 ($\rho$=1.55%), 41% in S6 ($\rho$=0.91%), 64% in S7 ($\rho$=0.91%), 50% in S8 ($\rho$=0.91%), 53% in S9 ($\rho$=0.91%), or 51% in S10 ($\rho$=0.91%). Only in S3 ($\rho$=0.91%) with the lower strength steel (f_{yl}=320.5 MPa), the steel strain ($\varepsilon_{s,c}(t)$=1352 μ) reached 82% of the yield strain (ε_{yl}=1619 μ). Although the steel strains would increase more with time, based on the tendency, steel yielding is not likely to occur under further loading.

The low creep and shrinkage of concrete ($\phi_{cru,s}$ and $\varepsilon_{shu,s}$=1.60 and 475 μ for C30 or 0.85 and 320 μ for C80) were appeared to be the main reason for the unyielding of longitudinal bars in the column specimens having a reinforcement ratio less than the 1% requirement of ACI 318 (2014). Using the proposed equation of Kim and Gong (2018) (restated in Eq. (6) for reference), where ϕ_{cru}, ε_{shu}, and other critical design parameters can be directly considered in design, the minimum reinforcement ratio was calculated for the column specimens.

$$\rho_{\min} = \frac{\dfrac{P_{serv}/\beta_N}{A_g} \times \dfrac{(1+\phi_{cru})}{E_c} + \varepsilon_{shu} - \varepsilon_{yl}}{\varepsilon_{shu} + \varepsilon_{yl}\left[\dfrac{E_s}{E_c}(1+\phi_{cru}) - 1\right]} \times \beta_I \tag{6}$$

where β_N=0.8−2×e_0/D×(1−e_0/D)−0.0015λ; β_I=1 for all the column specimens; and ϕ_{cru} and ε_{shu}=ultimate creep coefficient and shrinkage strain.

Except in S3 ($\rho_{\min}$=0.36% from Eq. (6)), the minimum reinforcement was calculated as unnecessary (that is, longitudinal bars in the column specimens are not supposed to yield in service under the given conditions), which are consistent to the test results. In actual design, however, even if the minimum reinforcement is calculated as unnecessary from Eq. (6), it is recommended to provide more than 0.5% of longitudinal bars to prepare for accidental situations that are not considered in the design and also to secure the minimum ductility of RC columns (in lightly reinforced columns, early flexural cracking could occur by bending moment, which may result in a brittle failure (Kim and Park 2010).

5. Conclusions

To investigate the long-term behavior of RC columns subjected to sustained eccentric loading, long-term eccentric loading tests were conducted for 10 RC columns. Test parameters included the concrete compressive strength, reinforcement ratio, bar yield strength, eccentricity ratio, slenderness ratio, and loading pattern. Based on the experimental and numerical study results, the minimum reinforcement to prevent longitudinal bars from yielding in service was discussed. The major findings are summarized as follows.

• From the cylinder tests, the ultimate creep coefficient and ultimate shrinkage strain were evaluated as 1.60 and 475 μ for C30 or 0.85 and 320 μ for C80. The evaluated values were higher in the low-strength concrete (C30) than in the high-strength concrete (C80) as expected, and were smaller than the recommendation of ACI 209R-92 (2.35 and 780 μ).

• From the column tests, the gradual increase in strains and curvatures with time and the gradual force-redistributions from concrete to longitudinal bars were observed, which were caused by creep and shrinkage. In the control specimen S1, the steel strain, curvature, and steel force were increased by 168%, 150%, and 152% at t=188 days (160 days after loading), respectively.

• The long-term behavior of RC columns varied with the test parameters. Compared to S1 (f_c' = 24.5 MPa, f_{yl}=441 MPa, ρ=0.91%, λ=kL/r=31.9, e_0/D=0.3, $P_{serv}/P_{u,s}$=0.41, and 1-step loading), the long-term effect was much less pronounced in S2 with the higher strength concrete (f_c' = 63.3 MPa). In S3 with the lower strength steel (f_{yl}=320.5 MPa), the overall behavior was similar, but the steel strain was closer to the yield strain. The long-term effect was more pronounced in S4 with the lower bar ratio (ρ=0.60%), but smaller in S5 with the higher bar ratio (ρ=1.55%). The long-term effect was smaller in S6 with the two-step loading, because the concrete was subjected to lower stresses at early ages. In S7 with the lower eccentricity ratio (e_0/D=0.1), the increments in the steel strain and steel force were higher but the increment in the curvature was smaller, due to the lower eccentricity and higher compression. In S8 with the higher eccentricity ratio (e_0/D=0.5), the long-term effect was more significant even under the much lower service load (54% of S1). From S9 (λ=21.5) and S10 (λ=41.8), it can be observed that the long-term effect was increased with the increase of the second-order effect.

• Although there were some fluctuations in the actual service load and eccentricity ratio applied to the column specimens, the numerical analysis using the ultimate creep coefficient and ultimate shrinkage strain measured from the cylinder specimens gave quite good predictions (at the final measuring day, the mean and standard deviation of prediction-to-test ratios=0.92±0.34). This result indicates that, if concrete cylinder test results are available, the long-term behavior of RC columns can be predicted with reasonable precision.

• In all the column specimens, no longitudinal bars were yielded under service loads at the final measuring day. The measured steel strain was just 41% to 66% of the yield strain, except in S3 (82%) with the lower strength steel. The low creep and shrinkage of concrete were appeared to be the main reason for the unyielding of longitudinal bars in the column specimens having a reinforcement ratio less than the current 1% requirement.

Acknowledgments

This research was supported by grants from the National Natural Science Foundation of China (Research Fund for International Young Scientists, Grant No. 51650110498 and 51750410691) and the Research Program funded by the SeoulTech (Seoul National University of Science and Technology), and the authors are grateful to the authority for their supports.

References

ACI Committee 209 (1997), Prediction of Creep, Shrinkage, and Temperature effects in Concrete Structures (ACI 209R-92), American Concrete Institute, Farmington Hills, MI, USA.

ACI Committee 318 (2014), Building Code Requirements for Structural Concrete and Commentary (ACI 318), American Concrete Institute, Farmington Hills, MI, USA.

ACI Committee 501 (1936). "Building regulations for reinforced concrete", *J. Proc. Am. Concrete Inst.*, **32**(3), 407-444.

Architectural Institute of Korea (2016), Korean Building Code and Commentary (KBC), Seoul, Republic of Korea. (in Korean)

ASTM (2015), Standard Test Method for Creep of Concrete in Compression (ASTM C512/C512M), American Society for Testing and Materials, West Conshohocken, PA, USA.

ASTM (2016), Standard Test Methods for Tension Testing of Metallic Materials (ASTM E8/E8M), American Society for Testing and Materials, West Conshohocken, PA, USA.

ASTM (2018), Standard Test Method for Compressive Strength of Cylindrical Concrete Specimens (ASTM C39/C39M), American Society for Testing and Materials, West Conshohocken, PA, USA.

B-Jahromi, A., Rotimi, A., Tovi, S., Goodchild, C. and Rizzuto, J. (2017), "Evaluation of the influence of creep and shrinkage determinants on column shortening in mid-rise buildings", *Adv. Concrete Constr.*, **5**(2), 155-171. https://doi.org/10.12989/acc.2017.5.2.155.

Bradford, M.A. (2005), "Shrinkage and creep response of slender reinforced concrete columns under moment gradient: theory and test results", *Mag. Concrete Res.*, **57**(4), 235-246. https://doi.org/10.1680/macr.2005.57.4.235.

Claeson, C. and Gylltoft, K. (2000), "Slender concrete columns subjected to sustained and short-term eccentric loading", *ACI Struct. J.*, **97**(1), 45-53.

Eom, T.S., Kim, C.S., Zhang, X. and Kim, J.Y. (2018), "Time-dependent deformations of eccentrically loaded reinforced concrete columns", *Int. J. Concrete Struct. Mater.*, **12**(76), 1-12. https://doi.org/10.1186/s40069-018-0312-1.

European Committee for Standardization (2008), Eurocode 2: Design of Concrete Structures – Part 1-1: General Rules and Rules for Buildings (Eurocode 2), European Committee for Standardization; Brussels, Belgium.

Gilbert, R.I. (1988), *Time Effects in Concrete Structures*, Elsevier Science Publishing Company Inc., New York, USA.

Green, R. and Breen, J.E. (1969), "Eccentrically loaded concrete columns under sustained load (including Part 2. Supplement)", *ACI J., Proc.*, **66**(11), 866-874.

Hamed, E. and Lai, C. (2016), "Geometrically and materially nonlinear creep behaviour of reinforced concrete columns", *Struct.*, **5**, 1-12. http://dx.doi.org/10.1016/j.istruc.2015.07.001.

Huo, X.S., Al-Omaishi, N. and Tadros, M.K. (2001), "Creep, shrinkage, and modulus of elasticity of high-performance concrete", *ACI Mater. J.*, **98**(6), 440-449.

Kataoka, L.T. and Bittencourt, T.N. (2014), "Numerical and experimental analysis of time-dependent load transfer in reinforced concrete columns", *Ibracon Struct. Mater. J.*, **7**(5), 747-774. http://dx.doi.org/10.1590/S1983-41952014000500003.

Kim J.K. (2003), "Creep tests for CFT columns I – Study on long-term behavior of CFT columns with diaphragm", *Seminar on Construction Technology for CFT Structures*, Architectural Institute of Korea, Seoul, Republic of Korea. (in Korean)

Kim, C.S. and Gong, Y. (2018), "Numerical investigation of creep and shrinkage effects on minimum reinforcement of concentrically and eccentrically loaded RC columns", *Eng. Struct.*, **174**, 509-525. https://doi.org/10.1016/j.engstruct.2018.07.032.

Kim, C.S. and Park, H.G. (2010), "Longitudinal reinforcement ratio for performance-based design of reinforced concrete columns", *J. Korea Concrete Inst.*, **22**(2), 187-197. https://doi.org/10.4334/JKCI.2010.22.2.187. (in Korean)

Kim, C.S., Park, H.G., Choi, I.R. and Chung, K.S. (2017), "Effect of sustained load on ultimate strength of high-strength composite columns using 800 MPa steel and 100 MPa concrete", *J. Struct. Eng.*, ASCE, **143**(3), 04016189-1-16. https://doi.org/10.1061/(ASCE)ST.1943-541X.0001676.

Kim, H.S. and Shin, S.H. (2014), "Reduction of differential column shortening by placing additional reinforcement", *Mag. Concrete Res.*, **66**(9), 456-464. http://dx.doi.org/10.1680/macr.13.00319.

Kordina, K. (1972), Langzeitversuche an Stahlbetonstützen. Institut für Baustoffkunde und Stahlbetonbau, Braunschweig, German. (in German)

Lou, T., Lopes, S.M.R. and Lopes, A.V. (2015), "FE analysis of short- and long-term behavior of simply supported slender prestressed concrete columns under eccentric end axial loads causing uniaxial bending", *Eng. Struct.*, **85**, 52-62. https://doi.org/10.1016/j.engstruct.2014.12.023.

Ministry of Housing and Urban-Rural Construction of the People's Republic of China (2015), National Standard of the People's Republic of China - Code for Design of Concrete Structures (GB 50010), China Architecture & Building Press, Beijing, P.R. China. (in Chinese)

New Zealand Standard (2017), Concrete Structures Standard: Part 2 – Commentary on the Design of Concrete Structures (NZS 3101-2), Standards New Zealand, Wellington, New Zealand.

Sun, G.J., Xue, S.D, Qu, X.S. and Zhao, Y.F (2019), "Experimental investigation of creep and shrinkage of reinforced concrete with influence of reinforcement ratio", *Adv. Concrete Constr.*, **7**(4), 211-218. https://doi.org/10.12989/acc.2019.7.4.211.

Tatsa, E.Z. (1989), "Load carrying of eccentrically loaded reinforced concrete panels under sustained load", *ACI Struct. J.*, **86**(2), 150-155.

Viest, I.M., Elstner, R.C. and Hognestad, E. (1956), "Sustained load strength of eccentrically loaded short reinforced concrete columns", *J. Am. Concrete Inst.*, **27**(7), 727–755.

Ziehl, P.H., Cloyd, J.E. and Kreger, M.E. (1988), "Evaluation of minimum longitudinal reinforcement requirements for reinforced concrete columns", Research Report 1473-S, Center for Transportation Research, University of Texas at Austin, TX, USA.

JK